Spin density in YTiO_{3}: I. Joint refinement of polarized neutron diffraction and magnetic x-ray diffraction data leading to insights into orbital ordering

I. A. Kibalin, Z. Yan, A. B. Voufack, S. Gueddida, B. Gillon, A. Gukasov, F. Porcher, A. M. Bataille, F. Morini, N. Claiser, M. Souhassou, C. Lecomte, J.-M. Gillet, M. Ito, K. Suzuki, H. Sakurai, Y. Sakurai, C. M. Hoffmann, and X. P. Wang

Phys. Rev. B **96**, 054426 — Published 21 August 2017

DOI: 10.1103/PhysRevB.96.054426

Spin density in $YTiO_3$ part I: Joint refinement of polarized neutron diffraction (PND) and magnetic X-ray diffraction (XMD) data, a new insight on the orbital ordering

I.A. Kibalin[1,2,4], Z.Y. Yan[3], A.B. Voufack[4], S. Gueddida[3], B. Gillon[1,*], A. Gukasov[1], F. Porcher[1], A.M. Bataille[1], F. Morini[4], N. Claiser[4], M. Souhassou[4], C. Lecomte[4], J. M. Gillet[3], M. Ito[5], K. Suzuki[5], H. Sakurai[5], Y. Sakurai[6], C.M. Hoffmann[7], and X.P. Wang[7]

[1] *Laboratoire Léon Brillouin, CEA-CNRS, CE-Saclay, 91191Gif-sur-Yvette, France*

[2] *PNP NRC "Kurchatov Institute" Orlova rosha, Gatchina, 188300 Leningrad region, Russia*

[3] *Laboratoire SPMS, UMR 8580, CentraleSupélec, 92295 Chatenay-Malabry, France*

[4] *CRM2, Institut Jean Barriol, University of Lorraine and CNRS, Vandoeuvre-les-Nancy, BP239, F54506, France*

[5] *Graduate School of Science and Technology, Gunma University, 1-5-1 Tenjin-cho, Kiryu, Gunma 376-8515, Japan*

[6] *Japan Synchrotron Radiation Research Institute (JASRI), SPring-8,1-1-1 Kouto, Sayo, Hyogo 679-5198, Japan and*

[7] *Chemical and Engineering Materials Division, Oak Ridge National Laboratory, 1 Bethel Valley Road, Oak Ridge, TN 37831, USA**

(Dated: July 10, 2017)

Orbital ordering below 30 K was previously observed in the ferromagnetic $YTiO_3$ compound both by polarized neutron diffraction (PND) and X-ray magnetic diffraction (XMD). In this paper we report a new procedure for the joint refinement of a unique spin density model based on both PND and XMD data. The distribution of the unpaired 3d-electron of titanium is clearly seen on the magnetization density reconstructed by the Maximum of Entropy Method from the PND data collection at 5 K. The Ti^{3+} 3d orbital populations obtained by joint model refinement are discussed in terms of the orbital ordering scheme. Small but significant magnetic moments on apical oxygen O_1 and yttrium atoms are found. The agreement between experimental and theoretical spin densities obtained using density functional theory is discussed.

Keywords: polarized neutron diffraction, X-ray magnetic diffraction, orbital ordering, YTiO3, perovskites

I. INTRODUCTION

Among the titanates presenting a pseudocubic perovskite structure and showing orbital ordering phenomenon, the perovskite-type $YTiO_3$ crystal has drawn considerable attention because of the existence of antiferromagnetic orbital ordering in the ferromagnetic state. $YTiO_3$ is a ferromagnetic insulator with a Curie temperature of 30 K. It has been investigated theoretically [1–3] and by various experimental techniques such as Nuclear Magnetic Resonance [4], polarized and unpolarized neutron diffraction [5 and 6], inelastic neutron scattering [7], resonant X-ray scattering [8], soft X-ray linear dichroism [9], X-ray magnetic diffraction [10], Compton scattering [11] and elastic X-ray scattering [12]. Theoretical studies using unrestricted Hartree-Fock calculation and Density Functional Theory (DFT) with generalized gradient approximation predicted the wave functions of orbital ordering state of the 3d electrons of Ti atoms to be the linear combination of $|yz\rangle$ and $|xz\rangle$ orbitals of t_{2g} state [1].

The first direct evidence of orbital ordering in $YTiO_3$ has been given by J. Akimitsu et al. [6] by using the polarized neutron diffraction (PND) technique. Experimental magnetic form factors of "special" reflections originating from the aspherical contribution of the Ti spin density were measured. It was noted that these magnetic reflections are forbidden in the spherical approximation for magnetic structure factor calculations. An appearance of magnetic response at these reciprocal points is directly related to the existence of the orbital ordering. Moreover, the measured magnetic form factors were confronted with a model of orbital ordered configuration of the t_{2g} electrons matching the symmetry of the Jahn-Teller distortion. It was found that the populations of the $|yz\rangle$ and $|xz\rangle$ orbitals in the t_{2g} state orbital functions, fitted from experimental results, are in agreement with the model [6].

The "antiferromagnetic" orbital ordering in $YTiO_3$ was also confirmed by X-ray magnetic diffraction (XMD) experiments [10 and 13]. The magnetic form factor obtained for a total of 62 reciprocal-lattice points was found in agreement with calculated one using the ordered orbital model mentioned above. Moreover, the XMD technique allowing the separation of orbital- (L) and spin- (S) form factors gave evidence for the total quenching of the orbital moment in $YTiO_3$ [10]. We note that PND and XMD methods are rather complementary: PND typically provides information on the magnetic form factor for scattering vectors with $\sin(\theta)/\lambda < 0.6\,\text{Å}^{-1}$ thus giving information about outer part of the spin distribution, while the XMD operating at $\sin(\theta)/\lambda > 0.3\,\text{Å}^{-1}$ is more sensitive to its inner part. Thus, a joint refinement of the PND and the XMD data may give a new insight on the spin distribution, hence, orbital ordering in $YTiO_3$.

Unfortunately, the PND data set reported in [6] is quite limited as it contains only zonal reflections ([0kl], [h0l] and [hk0]). Recent progress in polarized neutron diffraction technique due to the use of area detectors [14] and more efficient polarizers [15] as installed at LLB-Orphée

(Saclay) allow fast acquisition of flipping ratios in a large portion of the reciprocal space. Therefore a new series of flipping ratios measurements has been undertaken on $YTiO_3$ with the aim to achieve the highest possible data completeness and redundancy with a $0.6\,\text{Å}^{-1}$ resolution. High completeness was found to be very important not only in the model refinement but in particular when using a model-free analysis of data based on the reconstruction of the 3D spins distribution by the maximum entropy method (MEM). We used MEM reconstruction to uncover the presence of spin density on the ligands. Here we present the results of these new PND studies on $YTiO_3$ and the results of their joint treatment with XMD data.

This work is a part of a larger project which aims at developing a new model of the experimental spin-resolved electron density common to experimental techniques as different as high resolution X-Ray Diffraction (XRD), PND, XMD and Magnetic Inelastic Compton Scattering (M-ICS). Previous work has shown that spin-resolved electron density can be modelled using joint refinement against X-ray, neutron and polarized neutron diffraction data [16]. While PND gives access to the spin density in the position space, M-ICS permits to explore the spin density in the momentum space. The results thus obtained by M-ICS for $YTiO_3$ will be presented in a following paper (Part II) [17] and confronted to the present spin density in position space.

II. EXPERIMENTAL

A. Unpolarized neutron diffraction

A single crystal of $YTiO_3$ of size $(1\text{x}2\text{x}3.5)\,\text{mm}^3$ was used in all experiments. The crystal was provided by one of us. Prior to spin density studies, the nuclear structure was investigated at the hot neutron four-circle diffractometer 5C2 (LLB-Orphée, Saclay) using $\lambda = 0.84\,\text{Å}$. A total of 850 reflections up to $\sin\theta/\lambda = 0.60\,\text{Å}^{-1}$ were measured and 280 unique ones ($218 > 3\sigma$) were obtained by merging equivalents, using space group $Pnma$. In order to reveal possible deviations from the $Pnma$ symmetry in the ferromagnetic phase, data collections were performed at room temperature, in the paramagnetic phase at $\text{T} = 40\,\text{K}$ (above the Curie temperature T_C=30 K) and in the ferromagnetic phase at $\text{T} = 14\,\text{K}$. Since numerous reflections violating $Pnma$ special extinction rules were observed in these data sets, an *ab initio* structure determination was carried out on the single crystal diffractometer TOPAZ (Spallation Neutron Source, Oak Ridge) at $\text{T} = 90\,\text{K}$ and room temperature. At each temperature more than 5500 reflections (up to $\sin\theta/\lambda = 1.00\,\text{Å}^{-1}$) were measured. Details on the TOPAZ data collection are provided in Supplemental Material (Table 1S) [18].

B. PND

Magnetization density studies were performed at the thermal polarized neutron lifting counter diffractometer 6T2 (LLB-Orphée, Saclay) [15]. Neutrons of wavelength 1.4 Åwere monochromated by vertically focusing graphite crystal and polarized by a supermirror bender. The polarization factor of the beam was $p = 0.95$. In order to fully magnetize the sample, a 5 T magnetic field was applied. Data were collected at three different sample orientations, along the main crystallographic axes a, b, c respectively oriented parallel to magnetic field. Flipping ratios R_{PND} [Eq. (1)], i.e. the ratios between the spin-up and spin-down intensities of more than 260 (hkl) reflections were measured in the ferromagnetic phase at 5 K:

$$R_{PND} = \frac{y^+}{y^-} \cdot \frac{F_N^2 + 2pq^2F_NF_M + q^2F_M^2}{F_N^2 - 2peq^2F_NF_M + q^2F_M^2}. \qquad (1)$$

F_M and F_N denote the magnetic and nuclear structure factors. $q = \sin\alpha$ is a geometric factor with α being the angle between the scattering and the magnetization vector. e is the flipping efficiency. The parameters $y^{\pm}$ are extinction coefficients [see Eq. (4)].

Additional measurements with polarized neutrons have been carried out on the hot neutron spin polarized two axis diffractometer 5C1 (LLB-Orphée, Saclay). Neutrons from the source are monochromated and polarized by the (111) reflection of a magnetized Heusler crystal Cu_2MnAl. The wavelength is 0.84 Å, which corresponds to the maximum flux of the hot source and it is ideal for studying large domains of reciprocal space. The polarization factor of the beam is $p = 0.90$. A magnetic field of $H = 5\,\text{T}$ was applied along the axis c. The flipping ratios for over 110 (hkl) observed reflections with l=0,1,2,3,4 have been measured at $T = 5\,\text{K}$.

C. XMD

In the joint refinement and MEM reconstructions we used the data from XMD experiment performed earlier on the BL3C3 beamline of the Photon Factory of KEK in Tsukuba, Japan [10 and 13]. These measurements were made at 15 K with a magnetic field of 0.85 T, which is sufficient to saturate the magnetization along any axis in the bc plane [19]. The flipping ratios were measured for 47 independent reflections:

$$R_{XMD} = \frac{I_+ - I_-}{I_+ + I_-} = \gamma f_P \frac{F_{MS}}{F_{ch.}} \sin\theta. \qquad (2)$$

Here I_+ and I_- are the scattering intensity before and after the magnetization reversal, γ is the energy factor given as $\gamma = \hbar\omega/mc^2$ where $\hbar\omega$ is energy of X-rays and mc^2 is the electron rest mass energy, f_P is the polarization factor, F_{MS} and $F_{ch.}$ are the spin part of magnetic

TABLE I. Structure parameters of $YTiO_3$ at 40 K from structural refinement on 280 unique reflections with obtained agreement R-factor of 0.03.

Atom	x	y	z	B_{iso} (Å^2)
Y	0.0739(1)	0.25	0.9780(1)	0.24(1)
Ti	0.5	0	0	0.17(2)
O_1	0.4577(1)	0.25	0.12081(7)	0.28(1)
O_2	0.3093(1)	0.05801(5)	0.69042(8)	0.29(1)
$a = 5.6844(31)$Å, $b = 7.5873(44)$Å, $c = 5.3104(47)$Å				

structure factor and the charge structure factor, respectively, and θ is the Bragg angle set to 45° for that experiment.

It should be noted that the *Pbnm* space group, equivalent to *Pnma*, was used for the description of $YTiO_3$ crystal structure in [10 and 13]. In the present paper the standard *Pnma* space group is used.

III. RESULTS

A. Nuclear structure and extinction

The integrated intensities measured on 5C2 at 40 K and 300 K were used for the structural refinement in *Pnma* space group. The refinement process includes the atomic positions and isotropic temperature parameters plus six additional extinction parameters according to an anisotropic extinction model implemented in FullProf [20]. The extinction is described by the y_{hkl} coefficient which gives a relation between the experimentally measured intensity of Bragg reflection, I_{exp}, and the intensity I_0, "corrected" for extinction:

$$I_{exp.} = y_{hkl} \cdot I_0. \tag{3}$$

This coefficient is expressed as a scalar function of the extinction parameter q_{hkl}, the wavelength λ, the structure factor F_{hkl}, and the diffraction angle 2θ:

$$y_{hkl} = \frac{1}{\sqrt{1 + 2.5 \cdot 10^{-4} \cdot \frac{q_{hkl} F_{hkl}^2 \lambda^3}{\sin 2\theta}}}, \tag{4}$$

with $q_{hkl} = (q_1 h^2 + q_2 k^2 + q_3 l^2 + q_4 hk + q_5 hl + q_6 kl) \cdot (\lambda / \sin\theta)^2$ and q_1,..., q_6 as refinable parameters. An accurate description of extinction effects has crucial importance for polarized neutron diffraction measurements because extinction has very strong influence both on unpolarized diffraction intensity and on flipping ratio used for the determination of magnetic structure factor [Eq.(1)].

The refinement results are given in Table I for data measured at 40 K in the paramagnetic phase. The anisotropic thermal parameters are provided in Supplemental Material (Table 2S) [18]. The obtained structure

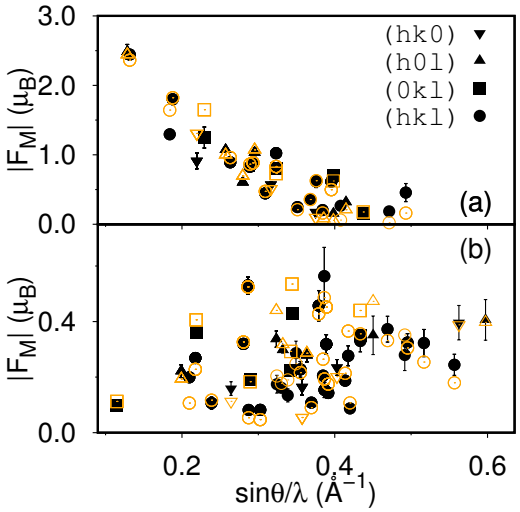

FIG. 1. (Color online) Observed (filled symbols) and calculated (open symbols) modulus of magnetic structure factors as a function of $\sin\theta/\lambda$ for PND data. Only unique reflections with non zero (a) and zero (b) contribution of spherical part of magnetic density of titanium into magnetic structure factor are shown.

parameters are in agreement with literature [12, 21, and 22]. Data treatment without extinction correction leads to worsening the goodness of fit by a factor of 20. Extinction parameters obtained in the refinement do not show any considerable dependence on the temperature.

To exclude a possible lowering of *Pnma* symmetry due to the orbital ordering, detailed structure studies were performed on the single crystal diffractometer TOPAZ at 90 K and room temperature. As in the 5C2 experiment, a certain number of weak reflections (about 350 at each temperature) violating *Pnma* extinction rules was found. However, detailed analysis of systematic absences and reflection conditions using SuperFlip program from JANA2006 [23] confirms the *Pnma* space group as described in Supplemental Material [18]. We believe that the observation of some systematically absent reflections in neutron diffraction is attributable to multiple scattering effects as observed in previous X-Ray diffraction experiments [12].

B. Magnetization density reconstruction

Nuclear structure factors and extinction parameters deduced from the unpolarized neutron experiments were used to derive the magnetic structure factors by solving Eq. (1).

Since the crystal structure is centrosymmetric, the magnetization density can be directly reconstructed from the measured magnetic structure factors by a model-free MEM [24]. Figure 2(a) shows the reconstructed three-dimensional magnetization density when all measured magnetic structure factors are included in the recon-

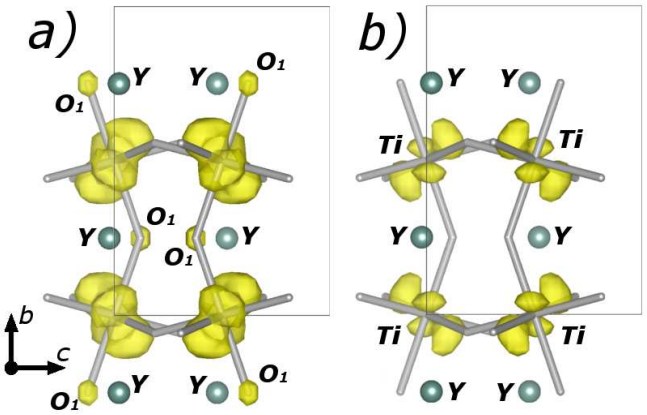

FIG. 2. (Color online) Magnetization density reconstructed by maximum entropy method with (a) all measured reflections (the level of isodensity surface is $0.05\,\mu_B/\text{Å}^3$) and (b) "special" reflections originating from the aspherical contribution of the Ti spin density distribution (the level of isodensity surface is $0.10\,\mu_B/\text{Å}^3$).

struction procedure. The antiferromagnetic ordering of 3d-orbitals in $YTiO_3$ compound is clearly seen in the figure 2(a). The lobes of the 3d-orbitals become even more pronounced if the density reconstruction is performed by using only "special" reflections for which the contribution of spherical part of magnetic density of titanium into magnetic structure factor is equal to zero(see figure 2(b), the number of reflections is 190). Such a reconstruction of spin density based on "special" reflections measured by XMD technique was used previously [25].

We also note that the magnetization density depicted in figure 2(a) shows weak magnetic density contributions located near the apical oxygen O_1 in $4c$ position. Summation of the density around each atom provides a rough estimate of magnetic moments. The magnetic moment of each atom is the following: $0.743\mu_B$ for titanium, $0.035\mu_B$ for oxygen O_1 , $0.021\mu_B$ for oxygen in general position O_2 and $-0.044\mu_B$ for yttrium.

C. Spin density model refinement of PND and XMD data

In this refinement, the magnetic structure factors are calculated from the spin density, which is modeled as a superposition of the spin densities of titanium, oxygen and yttrium atoms [26]. In the case of titanium atoms the spin density is estimated as the square of the modulus of the wavefunction of unpaired electron as described in the restricted Hartree-Fock method [24]. In this method the wave function is considered as a linear combination of Slater-type atomic functions:

$$\psi = \sum_{L=0}^{N-1} R_L(n_L, \xi_L, r) \sum_{M=-L}^{L} \alpha_{LM} Y_{LM}(\theta, \phi), \qquad (5)$$

TABLE II. Atomic magnetic moments (in μ_B) and titanium 3d orbital populations in ferromagnetic $YTiO_3$ from orbital model refinement with PND, XMD and joint PND-XMD data for two weighting schemes (see text).

	PND	XMD	Joint PND-XMD	
			scheme 1	scheme 2
Ti (μ_B)	0.715(4)	0.597(47)	0.713(4)	0.708(5)
$P(xy)$	0.0	0.0	0.0	0.0
$P(xz)$	0.39(3)	0.53(4)	0.44(2)	0.47(2)
$P(yz)$	0.61(6)	0.43(6)	0.55(4)	0.51(4)
$P(z^2)$	0.001(1)	0.03(1)	0.010(3)	0.022(4)
$P(x^2-y^2)$	0.0005(7)	0.003(3)	0.0000(1)	0.0000(1)
O_1 (μ_B)	0.016(4)	0.05(4)	0.013(4)	0.009(5)
O_2 (μ_B)	0.004(3)	-0.08(4)	0.005(3)	0.005(4)
Y (μ_B)	-0.047(4)	-0.14(4)	-0.049(4)	-0.053(5)
N_{obs}	286	62	348	348
GOF	5.3	3.5	5.4	5.6

where the values N, L and M are the quantum numbers (N is the principal quantum number; L is the azimuthal quantum number, M is the magnetic quantum number); $R_L(n_L, \xi_L, r)$ is the Slater-type radial function and $Y_{LM}(\theta, \phi)$ is the real spherical harmonics [26]. Coefficients α_{LM} are the atomic orbital coefficients with the normalisation condition. The wave function of an unpaired 3d electron of titanium Ti^{3+} has been refined with the following parameters: $N = 3$, $n_L = 2$, $\xi = 2.7$ and non zero coefficients α_{LM} at $L = 2$ [27].

The real spherical harmonics are defined in a local Cartesian coordinate system belonging to each titanium atom (see Figure 1S in SI). The local axes point to neighbouring oxygens. The z axis is directed towards the $O_2^{'}$ atom, which is farest from titanium (2.08 Å). The x axis is directed towards the O_1 atom. The y axis has a direction towards the O_2 atom. Distances from titanium to O_1 and O_2 atoms approximately equal to 2.02 Å.

For the description of spin density on the oxygen and yttrium atoms, the spherical model has been applied:

$$\rho_{sph.}(r) = \frac{1}{4}\pi \cdot \mu \cdot R_L(n_L, \xi_L, r), \qquad (6)$$

where μ is the atomic magnetic moment. Slater-type radial function has parameters: $n_L = 2$, $\xi_L = 4.45$ for oxygen and $n_L = 6$, $\xi_L = 7.98$ for yttrium [27].

The applied procedure is more universal for refinement of experimental data than the analytical expressions used previously [6 and 10]. More details about the model refinement of the spin density are available in literature [24].

The PND data refinement gives good agreement between calculated and experimentally observed flipping ratios (figure 1). The parameters of the model are listed in table II. The refined wave function of the unpaired electron of titanium in the asymmetric unit is:

$$\psi = \sqrt{0.61(6)}\,|yz\rangle + \sqrt{0.39(3)}\,|xz\rangle\,, \qquad (7)$$

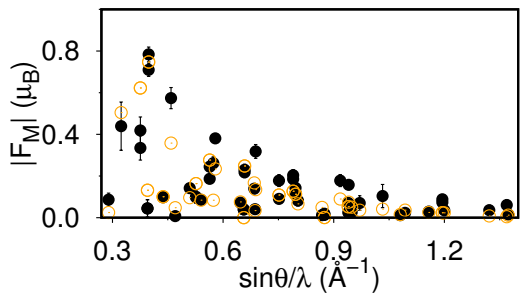

FIG. 3. (Color online) Observed (filled symbols) and calculated (open symbols) modulus of magnetic structure factors as a function of $\sin\theta/\lambda$ for XMD data.

where 3d-orbitals $|yz\rangle$ and $|xz\rangle$ are described by the real spherical harmonics $Y_{2-1}(\theta,\phi)$ and $Y_{2+1}(\theta,\phi)$, respectively.

We applied our refinement procedure to the experimental XMD data. The comparison between calculated and experimentally measured magnetic structure factors is shown on figure 3. Similar parameters of the model have been obtained (column 3 in table II).

In spite of a smaller number of reflections in case of XMD experiment compared to the PND one (62 points against 286 points), the refinement gives a similar distribution of the upaired 3d-electron of titanium and thus comparable information about antiferro-magnetic orbital ordering phenomenon. The error bars of magnetic moments of atoms are high because of the absence of reflections with low momentum transfer. The XMD data are restricted to the high momentum transfer reflections ($\sin\theta/\lambda > 0.3$ Å), for which a magnetic scattering is highly reduced due to the decrease of magnetic form factor versus resolution. For the same reason, introducing magnetic moments on oxygen and yttrium atoms does not significantly improve refinement of XMD data.

For the joint refinement of magnetic structure factors two weighting schemes were used. The first scheme minimizes the sum of the goodness-of-fit of each experiment [16, 28, and 29]. This weight usually favours the experiment that provides a large data set. The refinement results performed by the scheme are presented in column 4 of table II.

The second weighting scheme is based on the minimization of the sum of the goodness-of-fit normalized per data number for each experimental technique. It reduces the weighting ratio between large and small data sets and hence should better take into account the contribution of the small data set. The results are given in column 5 of table II. Both weighting scheme give the same results, not statistically different from PND only.

The population of 3d orbitals is in agreement with our XRD measurements performed at 100 K [22], where similar population of $|xz\rangle$ and $|yz\rangle$ orbitals were observed. The 3d electron lobes orientations of titanium atom are similar for the static deformation density calculated from XRD measurements and reconstructed spin density (figure 4)

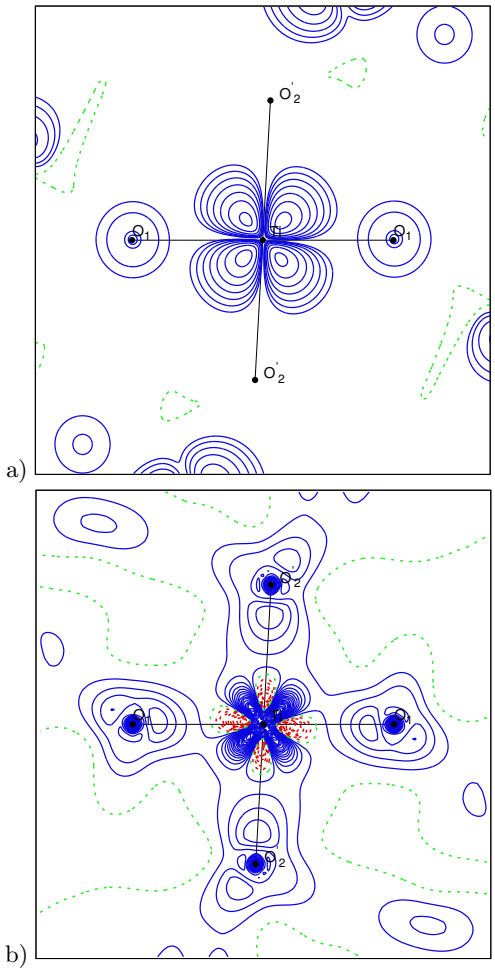

FIG. 4. (Color online) (a) Experimental spin density from joint PND-XMD model refinement (normalized to 1 per TiO_6 unit) in the $Ti-O_1-O_2^{'}$ plane. Contours at intervals of 0.01×2^n $(n=0,...,12)\mu_B\cdot$Å^{-3}, positive: blue lines, negative: red dashed lines and neutral: green dashed. (b) Static deformation density from X-ray diffraction at 100 K [22]. Contours at intervals of $0.1e\cdot$Å^{-3}, positive: blue lines, negative: red dashed lines and neutral: green dashed.

In addition to the magnetic moment on titanium atom, small magnetic moments on oxygen O_1 and yttrium atom are observed. It should be noted that the presence of small magnetization on oxygen and yttrium may be related to our recent XRD measurements, where anisotropic accumulation of electrons around these atoms was observed [22].

D. DFT computations

Ab initio computations based on density function theory (DFT) were done for $YTiO_3$ to compare with experiment. The computations were performed by the Crystal

TABLE III. Theoretical atomic spin populations in $YTiO_3$ in frame of Bader model (in e-) and Ti 3d-orbital populations (normalized to 1).

Bader spin population		3d-orbital population of Ti atom	
Ti	0.852	$P(xy)$	0.0
O_1	0.036	$P(xz)$	0.46(1)
O_2	0.049	$P(yz)$	0.54(2)
Y	0.015	$P(z^2)$	0.002(1)
		$P(x^2-y^2)$	0.0000(1)

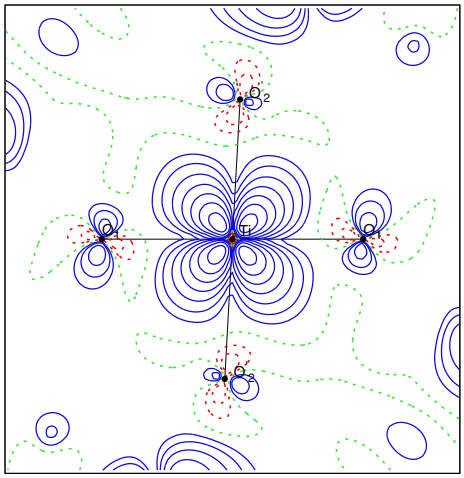

FIG. 5. (Color online) Spin density in the $Ti-O_1-O_2^{'}$ plane calculated by DFT. Contours at intervals of 0.01×2^n $(n = 0, ..., 12)\mu_B \cdot$Å^{-3}, positive: blue lines, negative: red dashed lines and neutral: green dashed.

14 package [30], which is optimized for periodic calculations. The calculations were carried out at the density functional theory level, using PBE0-1/3 [31] hybrid functional and optimized basis set proposed in [32 and 33]. One unpaired electron per Ti atom was attributed as initial guess. The theoretical spin populations obtained by Bader analysis performed by the TOPOND package [34] are presented in Table III. The theoretical 3d-orbital populations reported in Table III were estimated by applying the previously defined orbital model refinement to the calculated magnetic structure factors.The calculated spin density in the $Ti-O_1-O_2^{'}$ plane is displayed in Figure 5 for comparison with the results of the model refinement on experimental data (figure 4(a)).

The population of 3d orbitals of titanium atom is well consistent with the experimental results (see tables II and III). The lobes of the 3d-orbitals as shown by figures 4(a) and 5 demonstrate identical orientation for experiment and theory.

Besides the spin population on titanium atom, the Bader analysis shows a small population on oxygen and yttrium atoms. The estimated spin population on oxygen O_1 atom (4.1% relative to the population on titanium), is in agreement with experimental magnetic moment 0.013(4) μ_B, which is 1.8(6)% relative to the titanium magnetic moment as obtained by PND-XMD joint refinement in scheme 1 (Table 4).

The DFT calculations show a non zero spin population on oxygen O_2, even larger than the O_1 population. However, no significant magnetic moment on O_2 atoms was observed from refinement of experimental data. The spin population on O_2 atom given by DFT calculation looks overestimated [35 and 36].

The small magnetic moment observed on oxygen O_1 in the $YTiO_3$ compound may be significant for the understanding the role of this atom in mediating magnetic interactions between neighbouring Ti coordination polyhedra. It is widely recognized that the magnetic interaction between the neighbouring Ti t_{2g} orbitals are governed by the super-exchange processes mediated by the O 2p orbitals [1]. At that the t_{2g} bandwidth is reducing with decreasing the Ti-O-Ti bond angle. Because the bond angle for the O_1 atom is smaller than for the O_2 atom: 140.3° versus 143.7°, the magnetic exchange between titanium atoms is expected to occur mainly through the O_1 atom. The negative spin density located on the yttrium atom could result from spin polarization due to the positive spin density on the O_1 atom of the two short $Y-O_1$ bonds (2.23 and 2.31 Å) of the Y surrounding.

It should be noted that DFT calculations do not evidence any spin population on yttrium atom, contrary to the PND data analysis which exhibits a negative spin population on this atom. Indeed DFT calculations generally provide a qualitative agreement with experimental spin densities from PND but do not allow to describe very fine details of the spin distribution, which requires a higher level of theory like the CASSCF method [37]. A recent article [38] confirms that, in case of a multireference system which corresponds to a single d electron that could occupy any d orbital, the CASSCF approach is proved to give better results than DFT.

E. Conclusion

The model free reconstruction by the Maximum Entropy Method of the magnetization density in the ferromagnetic $YTiO_3$ based on the PND measurements provides direct observation of orbital ordering of 3d-orbitals of titanium and the first observation of a magnetic moment on the oxygen atoms in 4c position of $Pnma$ space group. The joint model refinement of PND and XMD data shows that the titanium 3d electron wave function can be described by a combination of $|xz\rangle$ and $|yz\rangle$ orbitals. The positive spin population obtained on the O_1 atom is in agreement with DFT calculations and recent results of charge density studies [22]. The new PND-XMD joint refinement method opens the way to accurate spin density determination in transition metal compounds presenting an orbital contribution to the magnetization density.

ACKNOWLEDGMENTS

IK thanks the french national research agency ANR for financial support (MTMED project). ZY thanks CSC for PhD scholarship support. ABV thanks University of Lorraine for a PhD fellowship. Work performed at the ORNL Spallation Neutron Sources TOPAZ single-crystal diffractometer was supported by the Scientific User Facilities Division, Office of Basic Energy Sciences, US Department of Energy.

* beatrice.gillon@cea.fr

[1] M. Mochizuki and M. Imada, New J. Phys. **6**, 154 (2004).
[2] H. Sawada and K. Terakura, Phys. Rev. B **58**, 6831 (1998).
[3] J. Choukroun, Phys. Rev. B **84**, 014415 (2011).
[4] M. Itoh , M. Tsuchiya, Journal of magnetism and magnetic materials **226**, 874 (2001).
[5] C. Ulrich, S. Okamoto G. Khaliullin, M. Reehuis, A. Ivanov, H. He, Y. Taguchi, Y. Tokura, and B. Keimer, Phys. Rev. Lett. **89**, 167202 (2002).
[6] J. Akimitsu, H. Ichikawa, N. Eguchi, T. Miyano, M. Nishi, and K. Kakurai, J. Phys. Soc. Jpn. **70**, 3475 (2001).
[7] B. Li, D. Louca, B. Hu, J. L. Niedziela,J. Zhou, and J. B. Goodenough, J. Phys. Soc. Jpn. **83**, 084601 (2014).
[8] H. Nakao, Y. Wakabayashi, T. Kiyama, Y. Murakami, M. V. Zimmermann, J. P. Hill, D. Gibbs, S. Ishihara, Y. Taguchi, and Y. Tokura, Phys. Rev. B **66**, 184419 (2002).
[9] F. Iga, M. Tsubota, M. Sawada, H. B. Huang, S. Kura, M. Takemura, K. Yaji, M. Nagira, A. Kimura, T. Jo, T. Takabatake, H. Namatame, and M. Taniguchi, Phys. Rev. Lett. **93**, 257207 (2006).
[10] M. Ito, N. Tuji, F. Itoh, H. Adachi, E. Arakawa, K. Namikawa, H. Nakao, Y. Murakami, Y. Taguchi, and Y. Tokura, J. Phys.Chem. Solids **65**, 1993 (2004).
[11] N. Tsuji, M. Ito, H. Sakurai, K. Suzuki, K. Tanaka, K. Kitani, H. Adachi, H. Kawata, A. Koizumi, H. Nakao, Y. Murakami, Y. Taguchi, and Y. Tokura, J. Phys. Soc. Jpn. **77**, 023705 (2008).
[12] J.R. Hester, K. Tomimoto, H. Noma, F. P. Okamura, and J. Akimitsu, Acta Cryst. **B53**, 739 (1997).
[13] S. Tsuji: Graduate thesis, Gunma University (2004); H. Akiyama: Master thesis, Gunma University (2006).
[14] A. Gukasov, S. Rodrigues, J.-L. Meuriot, T. Robillard, A. Sazonov, B. Gillon, A. Laverdunt, F. Prunes and F. Coneggo, Physics Procedia **42**, 150-3 (2013).
[15] A. Gukasov, A. Goujon, J.-L. Meuriot, C. Person, G. Exil, and G. Koskas, Physica B: Condensed Matter **397**, 131 (2007).
[16] M. Deutsch, B. Gillon, N. Claiser, J.-M. Gillet, C. Lecomte, M. Souhassou, IUCrJ. **1**, 194 (2014).
[17] Z.Y. Yan, I. Kibalin, S. Gueddida, B. Gillon, A. Gukasov, A.-B. Bolivard Voufack, N. Claiser, Y. Sakurai, M. Brancewicz, M. Itou, M. Itoh, N. Tsuji, M. Ito, M. Souhassou, C. Lecomte, P. Cortona, J.-M. Gillet, submitted to PRB
[18] See Supplemental Material at [URL will be inserted by publisher] for details on data collection, refined structural parameters, crystal structures solution of $YTiO_3$, and definition of local coordinate system for different sites of titanium atoms.
[19] N.N. Kovaleva, A.V. Boris, P. Yordanov, A. Maljuk, E. Brucher, J. Strempfer, M. Konuma, I. Zegkinoglou, C. Bernhard, A. M. Stoneham, and B. Keimer, Phys. Rev. B **76** 155125 (2007).
[20] J. Rodriguez-Carvajal, Physica B. **192**, 55 (1993).
[21] A. C. Komarek, H. Roth, M. Cwik, W.-D. Stein, J. Baier, M. Kriener, F. Bouree, T. Lorenz, and M. Braden, Phys. Rev. B **75**, 224402 (2007).
[22] A.B. Voufack et al. (2017) private communication.
[23] L. Palatinus and G. Chapuis, J. Appl. Cryst. **40**, 786 (2007).
[24] B. Gillon and P. Becker, Magnetization densities in Material Science, in Modern Charge density analysis, Eds C. Gatti, P. Macchi, (Springer, Dordrecht, 2012).
[25] K. Suzuki, M. Ito, N. Tsuji, H. Adachi, H. Nakao, Y. Murakami, Y. Taguchi, Y. Tokura, E. Nishibori, and M. Sakata, Photon factory activity report 2007 **25**, 83 (2008).
[26] N. Hansen and P. Coppens, Acta Crystallographica **A34**, 909 (1978).
[27] E. Clementi and C. Roetti, Atomic data and nuclear data tables **14**, 177 (1974).
[28] M. Deutsch, N. Claiser, S. Pillet, Y. Chumakov, P. Becker, J.-M. Gillet, B. Gillon, C. Lecomte, M. Souhassou, Acta Cryst. **A68**, 675 (2012).
[29] J. A. K. Duckworth, B. T. M. Willis, and G. S. Pawley, Acta Cryst. **A25**, 482 (1969).
[30] C. Pisani, in *Quantum-mechanical ab-initio calculation of the properties of crystalline materials* (Springer, Berlin, 1996).
[31] C. A. Guido, E. Bremond, C. Adamo, and P. Cortona, J. Chem. Phys. **138**, 021104 (2013).
[32] A. Buljan, P. Alemany, and E. Ruiz, J. Phys. Chem. B **103**, 8060 (1999).
[33] A. Erba, K. E. El-Kelany, M. Ferrero, I. Baraille, and M. Rérat, Phys. Rev. B **88**, 035102 (2013).
[34] C. Gatti, V. R. Saunders, and C Roetti, J. Phys. Chem. **101**, 10686 (1994).
[35] K. Boguslawski, C.R. Jacob, and M. Reiher, Journal of chemical theory and computation **7**, 2740 (2011).
[36] C.R. Jacob and M. Reiher, Int. J. Quantum Chem. **112**, 3661 (2012).
[37] A.-B. Voufack, N. Claiser, C. Lecomte, S. Pillet, Y. Pontillon, B. Gillon, Z. Yan, J.-M. Gillet, M. Marazzi, A. Genoni and M. Souhassou, Acta Cryst B (2017) Special Issue, Philip Coppens tribute, in press.
[38] P.Verma and D.G. Truhlar, Physical Chemistry Chemical Physics **19(20)**, 12898 (2017).